scientific reports

Check for updates

OPEN

# Effects of humic acid on enhanced removal of lead ions by polystyrene-supported nano-Fe (0) nanocomposite

Luyao Wang[1,2], Shiqiang Wei[2] & Zhenmao Jiang[2]✉

**Polymer-supported nanozero-valent iron composites (D001-nZVI) were fabricated for the removal of lead ions from aqueous solutions by embedding nZVI into the porous polystyrene anion exchanger D001. Humic acid (HA) was selected as a model species because of its ubiquitous existence to gain insight into the influencing factors in the actual application process. The iron contents of the composites were approximately 11.2%, and the smallest ZVI particle size was ~ 5 nm. The experimental results showed that the effect of HA on the reduction of lead ions by D001-nZVI was a concentration-dependent process. At low HA concentrations, the surface-competitive adsorption of HA and $Pb^{2+}$ dominated; therefore, the removal efficiency of $Pb^{2+}$ by D001-nZVI decreased from 97.5 to 90.2% with an increasing HA concentration. When the HA concentration increased to 30 mg/L or more, the lead ions removal remained constant with the following possible cooperation mechanism: the competitive adsorption of HA and $Pb^{2+}$ on the nZVI surface and the well-dispersed particles were caused by electrostatic interactions between the HA coating and the nZVI surface. In addition, the adsorption complexation between HA and $Pb^{2+}$ also had a positive effect on the removal of $Pb^{2+}$ at higher concentrations of HA.**

Heavy metal pollution in water is a global issue, such as the pollution by lead ions. The International Agency for Research on Cancer (IARC) has classified Pb as a possible carcinogen to humans (Group 2B). Although the quantity of Pb is only 0.0016% in the crust of the Earth[1], serious Pb pollution mainly originates from industry, i.e., paint, battery, smelting, hardware, machinery, electroplating, cosmetics, hair dyes, glaze dishes. The Bulletin on Environmental Quality of China's Coastal Waters in 2015[2] showed that the emission rate of lead ions was 0.3%, higher than the allowed limitation in China; in addition, civil health incidents caused by lead pollutants have also attracted widespread attention, such as serious blood-lead poisoning incidents in China and India[3]. Therefore, deep lead decontamination is urgent and significant. Conventional technologies include chemical precipitation, flocculation, ion exchange, adsorption, and membrane separation[4]. At present, chemical precipitation or flocculation is available for removing high concentrations of Pb ions, but it is inefficient at trace levels; reverse osmosis (RO) membranes are competent for removing trace heavy metals, including Pb ions, but their high operational cost significantly limits their applicability. Therefore, it is necessary to develop a cost-effective technology.

In recent years, transition metal oxides or M(0) and their composites have been industrialized as efficient adsorbents for heavy metal or diverse contaminant removal from water, such as $ZrO_2$[5], Fe(0)[6] or Mn(IV)[7]. Since the 1990s, nanozero-valent iron (nZVI) has been widely used in water/soil pollution remediation due to its large specific surface area, strong reducing and adsorption-driven and environmentally friendly properties to remove contaminants[8,9], such as $NO_3^-N$[8,10,11], Cr(IV)[12], Pb(II)[13,14], As[15,16] and organic pollutants[17,18]. Wang[19,20] found that nZVI exhibited efficient $Pb^{2+}$ removal in solution with efficiencies of ~ 99.8% at pH = 5, which resulted from the strong chemical reduction by nZVI and the adsorption by subsequent iron oxide cooperation on the surface of the nZVI particles.

However, nZVI tends to agglomerate into larger particles spontaneously to reduce its surface energy during its preparation and application[21], thereby significantly reducing its active surface area and reactivity. To overcome these problems, nZVI was encapsulated onto a solid porous support or stabilized with a liquid dispersant to promote the dispersion of nZVI. Commonly used carriers are montmorillonite, bentonite[9,22], activated carbon[23],

[1]Institute of Land Engineering and Technology, Shaanxi Provincial Land Engineering Construction Group Co., Ltd, Xi'an 710075, China. [2]The Key Laboratory of Agricultural Resources and Environment in Chongqing, College of Resource and Environment, Southwest University, Chongqing 400716, China. ✉email: windring@swu.edu.cn

kaolinite[24], resin[25,26], etc., and liquid dispersants are mainly starch[27], Tween-20, polyacrylic acid (PAA)[28] etc. Our previous studies also showed that the microporous resin modified with a positively charged quaternary ammonium group was more favourable for forming smaller nZVI particles than most conventional carriers and led to a higher reduction activity for nitrate removal[29]. In addition, Chanthapon et al.[30] also found that nZVI particles showed a well-dispersed morphology using cation exchange resin as a carrier, which further favoured Pb removal. The composite performance of organic carrier-inorganic nanoparticles is affected by the solution pH[14,31], coexisting ions[32], and the properties of natural humus in the reaction system in practical applications. However, studies on the effects of humic acid are still rare and insufficient[33]. Humic acid (HA) widely exists in natural water and industrial effluents, and it contains versatile functional groups, such as carboxylic acid, phenol hydroxyl, alcohol hydroxyl, ketone, quinone and ester groups[34]. There are three possible interactions between HA, heavy metal ions and nZVI. The first is a complexation between HA and the heavy metal ions. The abundant functional groups in HA can form a complex with heavy metal ions, in particular Pb[35]. In addition, the possible competitive adsorption between HA and Pb ions is also prevalent on the surface of iron oxides in nZVI. Wang and his coworkers[36] also confirmed that the presence of competitive adsorption between HA and Cr(VI) led to a significant decrease in Cr(VI) removal when HA was added. Seunghun Kang[37] also indicated that there were dual electrostatic interactions and complexation between the acidic functional groups of HA and the goethite surface. Liu et al.[38] found that the adsorption of negatively charged HA on the surface of $Fe_3O_4$ resulted in overall negatively charged HA-$Fe_3O_4$, which effectively reduced the aggregation and further oxidation of $Fe_3O_4$ particles, thereby enhancing the adsorption of heavy metal ions, and the removal of $Hg^{2+}$ and $Pb^{2+}$ reached over 99%. Gupta and Nayak[39] found that the effect of HA on the removal of $Cd^{2+}$ by orange peel-$Fe_3O_4$ composites was related to the electrostatic attraction between the positively charged composites and negative-HA at pH < 7.

The current research mostly focuses on the effects of HA on the performance of bare nZVI materials, but immobilized nZVI, especially with cation exchange resin as supports, is rarely studied. HA shows different interactions with the resin carriers, nZVI, and heavy metals within nanopore environment of the matrix, supports, when polystyrene-based nZVI composites (denoted as D001-nZVI) are applied for Pb removal from water. To clarify the different mechanisms in this complex system, the interaction between HA and D001-nZVI, HA and $Pb^{2+}$ was investigated first. Then, the direction and extent of the influence of HA on the removal performance of $Pb^{2+}$ by D001-nZVI and the structure-related performance of D001-nZVI were analysed. In natural water, iron and nZVI-permeable reactive barriers frequently undergo long periods of HA adsorption and precipitation. Therefore, the present study aimed to evaluate nZVI performance in contaminated groundwater remediation under ambient conditions along with the investigation of the role of HA in the reduction of Pb(II) by nZVI particles. The results in this study may provide new insights into the application of nZVI composites in the detoxification of natural water.

## Materials and methods

**Materials.** All chemicals used in this study, namely, $FeCl_3{\cdot}6H_2O$, $NaBH_4$, NaOH, $PbCl_2$, and absolute ethyl ethanol, were all analytical reagent-grade or above. The support material is the macroporous cation exchanger D001, a polystyrene-divinylbenzene polymer matrix with sulfonic acid groups, purchased from Zhejiang Zhengguang Industrial Co., Ltd., China. Prior to use, it was rinsed with NaOH (5 wt%) and HCl (5 wt%), adjusted to a neutral pH with distilled water and dried at 40 °C for 24 h. All solutions were prepared with ultrapure water with a resistivity of 18.25 MΩ·cm. Humic acids were purchased from Tianjin Guangfu Technology Development Co., Ltd. and extracted from weathered coal. The HA sample was first dissolved in ultrapure water, and then the solution pH was adjusted to approximately 10 with 0.1 M NaOH. Afterward, the HA solution was ultrasonically treated for 2 h to fully dissolve it, and then the pH was adjusted to 7 with 0.1 M HCl. Finally, the HA solution was filtered through 0.45-μm membranes after being shocked for 24 h at room temperature. All prepared solutions were stored at 4 °C in the dark until further use[40].

**Preparation of D001-nZVIs.** Ultrapure water with a resistivity of 18.25 MΩ was purged with $N_2$ gas purging for at least 1 h at room temperature and used for the preparation of nZVI to avoid oxidation during the modification process. Dry D001 resin beads (0.5 g) were added to 70 mL of a 2.0 M $FeCl_3$ solution; after 12 h of rotation in an end-over-end shaker, the solid beads were obtained by filtration, rinsed five times with ultrapure water and then introduced into 70 mL $NaBH_4$ solutions with different concentrations. After a certain time, the preloaded $Fe^{3+}$ could be reduced in ZVI. The composites were freshly prepared before each experiment, and the materials used for structural characterization were dried in a vacuum oven at 40 °C for 24 h[40].

**HA adsorption.** D001 or the new synthesized D001-nZVI with the same amount of D001 was added into mixed solutions of different concentrations (0, 1, 2, 5, 10, 15, 20, 30, 50, and 100 mg/L) of HA and $Pb^{2+}$ (500 mg/L), then shaken at a constant temperature of 298 K for 12 h at 120 rpm via a shaking-bed in a thermostatic water bath. The HA contents in the solutions before and after the reaction were measured[40].

**$Pb^{2+}$ removal.** In all batch experiments, the dosages of the resin (D001) were set as 1.0 g/L. To investigate the performance of the lead ion removal by the nanocomposites, the beads were introduced into a 50 mL solution containing $Pb^{2+}$ (500 mg/L) and different concentrations (0, 1.0, 2.0, 5.0, 10, 15, 20, 30, 50, 100 mg/L) of HA. The suspension was stirred at 120 rpm at a constant temperature of 298 K for 8 h. Then, the contents of $Pb^{2+}$ and HA in the solution after the reaction were separately analysed[40].

Kinetic tests were carried out to establish the effect of the contact time on the removal process and to quantify the removal rate. After adding the immobilized nZVI, 0.1000 g D001 was added to a flask containing 100 mL of a mixed solution of $Pb^{2+}$ (500 mg/L) and different concentrations of HA (1, 5, 15, 40 mg/L), which was stirred

| Samples | D001/g | $FeCl_3$/M | $NaBH_4$/% | Restore time/min | Average iron loading/% |
|---|---|---|---|---|---|
| a | 0.05 | 2.0 | 3 | 15 | 8.98 |
| b | 0.05 | 2.0 | 3 | 30 | 9.91 |
| c | 0.05 | 2.0 | 4 | 15 | 9.50 |
| d | 0.05 | 2.0 | 4 | 30 | 11.20 |

**Table 1.** The iron content of the resin in different reductant concentration and reduction time.

at 298 K at a rate of 120 rpm. Moreover, the $Pb^{2+}$ removal by the composites in the absence of HA was assessed as a control. Then, the concentration of residual $Pb^{2+}$ in the solution was determined at regular time intervals by the methods described in the following section.

To monitor the concentration of $Pb^{2+}$ over time, the new D001-nZVI composite (D001 dosage: 0.0500 g) was added to 50 mL of $Pb^{2+}$ (500 mg/L) and different concentrations of HA (0, 1, 5, 15, 40 mg/L), and the reaction was terminated at 2, 5, 10, 15, 30, 45, 60, 90, 120, and 180 min, after which the D001-nZVI composites and the solution were immediately separated. The reaction solution was filtered through a 0.45 μm filter membrane to measure the concentration of $Pb^{2+}$ in the filtrate (recorded as A), and the filter membrane and the precipitate were digested with nitric acid to determine the concentration of $Pb^{2+}$ (recorded as B). After the reaction, the D001-nZVI composites were repeatedly eluted with 3 mol/L NaCl solution to detect the concentration of $Pb^{2+}$ in the eluent (recorded as C), and the eluted particles were digested with nitric acid and the digested solution (recorded as D). A, B, C and D correspond to the amount of $Pb^{2+}$ remaining in the solution after the reaction, the amount of precipitate formed by complexation of $Pb^{2+}$ with HA, the amount of ion exchange of $Pb^{2+}$ by carrier resin D001, and the amount of $Pb^{2+}$ reduced by nZVI, respectively. The total Pb concentration is calculated as $T_{Pb} = A + B + C + D$.

**Characterization.** Fourier transform infrared (FT-IR) spectra of HA were recorded at room temperature with a Spectrum GX spectrophotometer (Nicolet IS10). The microstructure and phase of the D001-nZVI composites before and after the reaction were measured by transmission electron microscopy (TEM, JEM 1200EX, Japan) and X-ray diffraction (XRD, Bruker D8). The cross-section of the D001-nZVI composites after vacuum-drying was observed by a bulk electron microscope (MicroDemo SZM45-B2).

**Analyses.** The $Pb^{2+}$ concentrations in the solutions were determined by a flame atomic absorption spectrophotometer (Beijing General Instrument Co., Ltd. TAS-900). Humic acid was determined spectrophotometrically by measuring the absorbance at λmax = 254 nm (Horiba JY Aqualog), and a standard curve was obtained to determine the residual concentration[40]. The XRD results were collected as binding energies and fitted using MDI Jade 6.0 software.

## Results and discussion

**Optimization of the preparation conditions of D001-nZVI.** The amounts of nZVI in D001-nZVI were closely related to the $NaBH_4$ concentration and the reduction time, as shown in Table 1. The amounts of nZVI increased significantly when the concentration of $NaBH_4$ and the reduction time were increased. The corresponding cross-sections of the D001-nZVI beads were also analysed by electron microscopy, and the results are shown in Fig. 1A. In the calculation from chemometrics, the $Fe^{3+}$ adsorbed onto the matrix was completely reduced by the $NaBH_4$ solution with a mass concentration of 0.05%. However, Fig. 1A shows that samples a, b and c still showed different shades of yellow ($Fe^{3+}$), which indicated that the reduction of Fe(III) not only required a stoichiometric amount of reducing agent but also had a strong relationship with the diffusion of the reducing agent.

The concentration gradient force was enhanced by increasing the reducing time and reductant concentration, which was beneficial for the complete reduction of $Fe^{3+}$from the outside to the inside of the polymeric support bead. Therefore, the D001-nZVI used in the following experiments in this study was prepared by adding 7 mL of 2 mol/L $FeCl_3$ per 0.05 g of D001, shaking for 12 h at 298 K and then carrying out its reduction by reacting with 7 mL of 4% $NaBH_4$ solution for 30 min. The TEM image further shows the embedded nZVI morphology (Fig. 1B). The bulk aggregated background was ascribed to the polymeric matrix, and similar results were also observed in our previous study, while the embedded particles were assigned to nZVI with a size of ca. 5–10 nm (Fig. 1C). The XRD analysis of D001-nZVI (Fig. 1B) revealed that the characteristic peak of Fe(0) appeared at 44.9°[41], which indicated the possible presence of Fe(0) nanoparticles inside the matrix.

**The reaction between HA and $Pb^{2+}$ or D001-nZVI.** To further elucidate the interaction of the HA species with the hybrid D001-nZVI, a series of comparison experiments was conducted. Figure 2A shows the possible removal of HA by $Pb^{2+}$ precipitation, D001-nZVI or binary D001-nZVI and $Pb^{2+}$, respectively. Clearly, negligible HA adsorption onto D001-nZVI was observed, which was attributed to two different components, i.e., the matrix D001 and the embedded nZVI. Specifically, the negatively charged HA species exhibited strong electrostatic repulsion with the sulfonic acid group ($-SO_3H$) of matrix D001. In addition, the adsorption of HA onto nZVI was also insignificant; the solution pH (pH = 5) was lower than the oxidation–reduction potential of iron oxide (pH = 7.9 ± 0.1), and the amount of iron oxides formed on the surface of nZVI was low, although the surface of iron oxide was positively charged[42]. This result was also confirmed by infrared spectroscopy analysis,

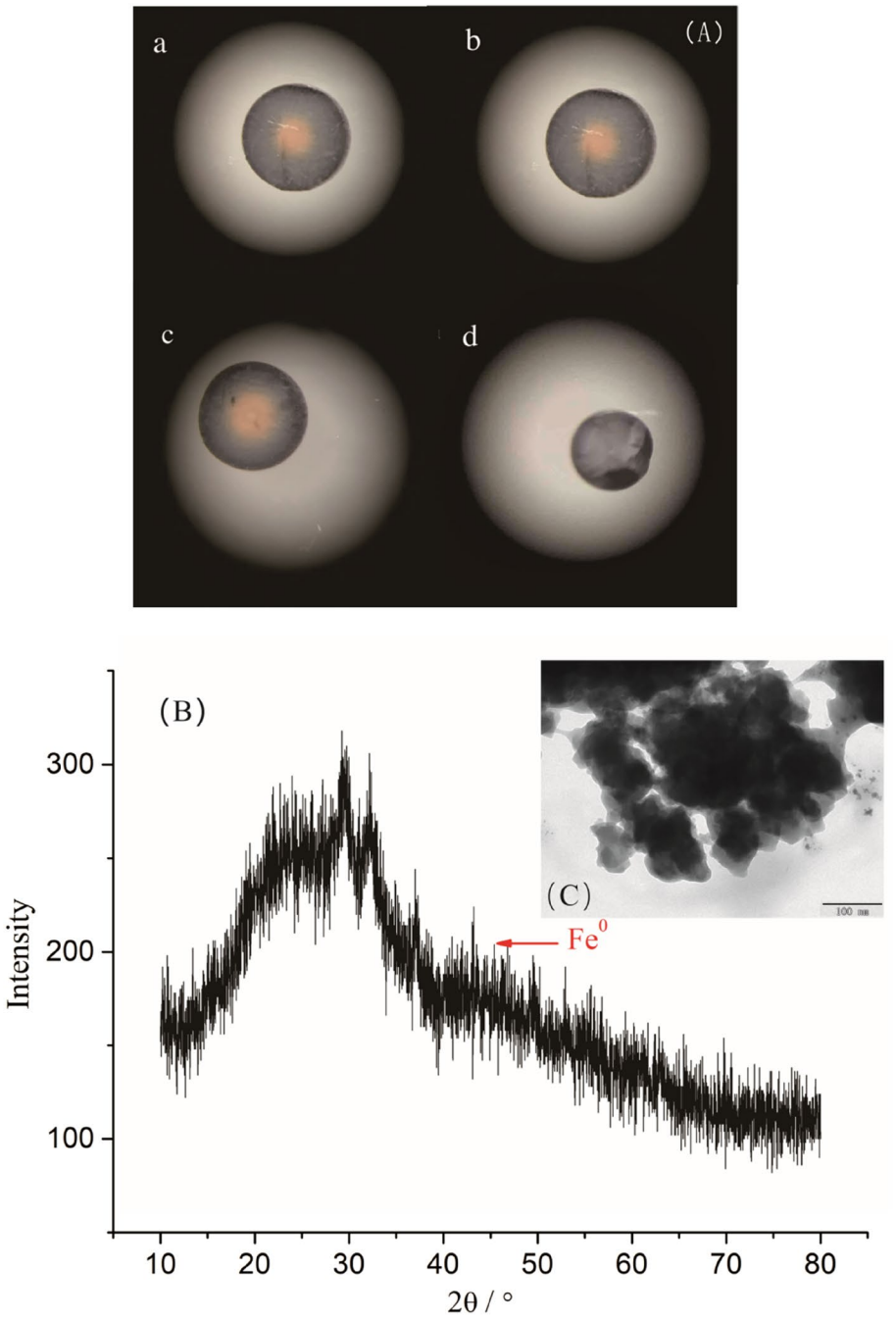


**Figure 1.** Micromorphology of D001-nZVI: (**A**) Micrograph of the D001-nZVI with different reducing agent concentrations and different reduction times; (**B**) TEM image of D001-nZVI; (**C**) XRD analysis of D001-nZVI.

as shown in Fig. 3. The major bands of HA appeared in the spectrum as follows: 3387.06 $cm^{-1}$ (O–H stretching of hydroxyl), 1033.75 $cm^{-1}$ (C–O stretching of primary alcohol), 1382.98 $cm^{-1}$ and 1599.86 $cm^{-1}$ (symmetric stretching of COO-, C–OH stretching of phenolic OH)[43]. Only the vibration of -OH (3447.52 $cm^{-1}$) was slightly shifted to 3449.62 $cm^{-1}$, which was attributed to the improved HA adsorption onto D001-nZVI.

Regarding the HA removal by $Pb^{2+}$ precipitation, the HA species readily formed complex precipitates with $Pb^{2+}$, and both $Pb^{2+}$ and HA could be removed from the solution as precipitates. It is noteworthy that HA removal remained constant when the added HA concentration was 10 mg/L or higher, which was ascribed to the complete complexation of Pb ions. Interestingly, the binary D001-nZVI and $Pb^{2+}$ systems exhibited favourable HA removal, indicating that HA can not only be complexed with $Pb^{2+}$ as precipitates but also be adsorbed by iron oxides on the outer surface of nZVI. The process was accompanied by the continuous formation of iron oxide, which occurred along with the $Pb^{2+}$ reduction by nZVI and further improved the adsorption of HA. Thus, the removal of HA by binary D001-nZVI and $Pb^{2+}$ was more efficient. In addition, HA may interact with the exterior

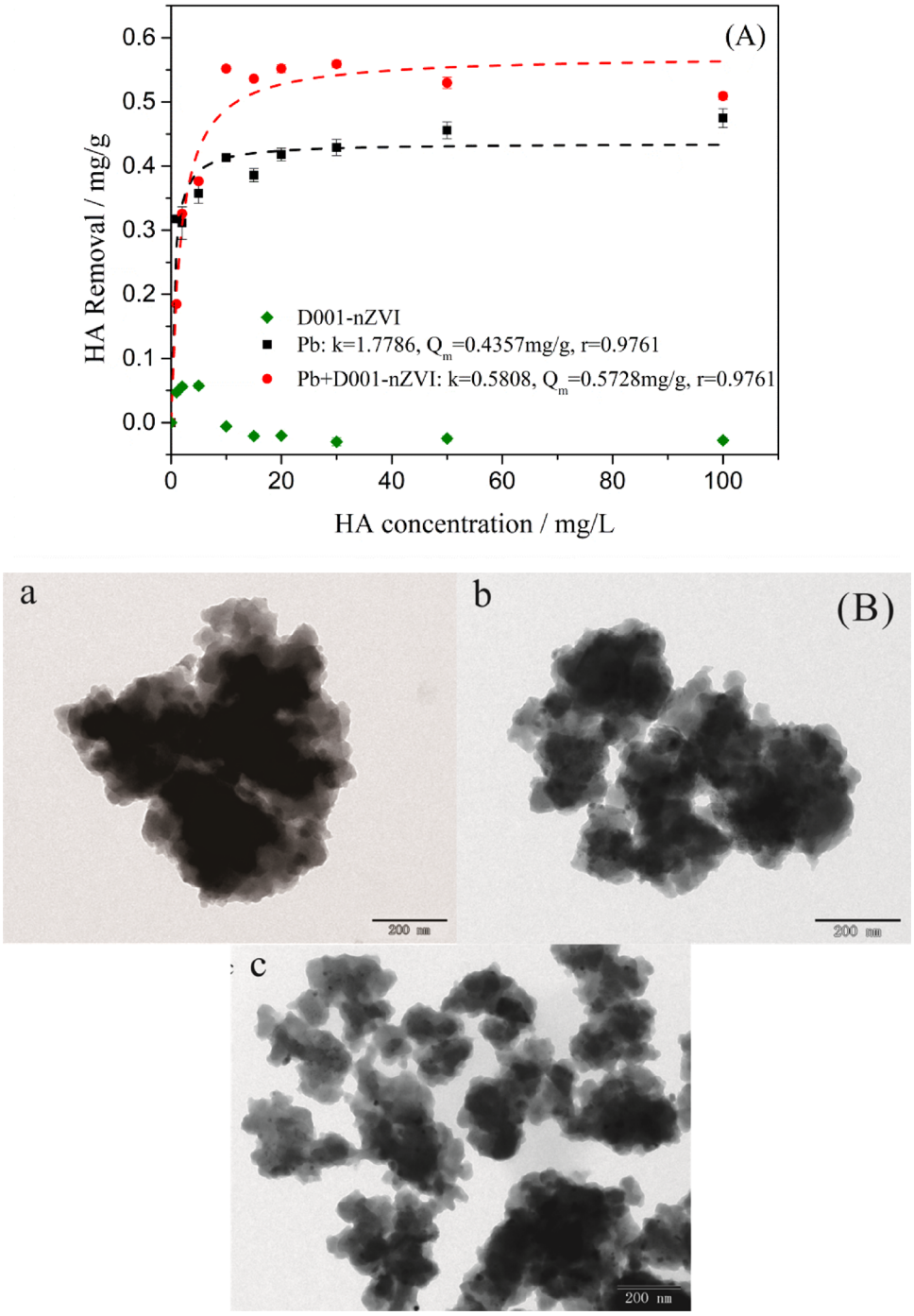


**Figure 2.** The adsorption characteristics of nZVI/ D001-nZVI and the TEM images before and after the reaction: (**A**) Adsorption isotherm of HA on D001, $Pb^{2+}$, and the coexistence system of D001-nZVI and $Pb^{2+}$; (**B**) TEM image of fresh D001-nZVI after reacted with (**a**) 0 mg/L, (**b**) 2 mg/L and (c) 100 mg/L HA (initial $Pb^{2+}$, 500 ppm; T, 298 K; initial pH, 7; ZVI for all the reaction mixtures was the same and equal to 11.20 Fe% in mass).

iron oxide of the nZVI shell, upon which the negative charge of HA can neutralize the positively charged iron oxide and generate a negatively charged nZVI surface by forming an organic macromolecular coating (hereinafter referred to as HA coating). The aggregation of the nZVI particles was inhibited by the electrostatic repulsion of the HA coating, which further increased the reactivity of nZVI[44]. The FTIR analysis of D001-nZVI after reacting with $Pb^{2+}$ before and after adding HA also confirmed this result. As shown in Fig. 3, the vibration of $-SO_3H$ (1041.13 $cm^{-1}$), the vibration of benzene (1632.21 $cm^{-1}$) and the vibration of –OH (3452.62 $cm^{-1}$) in D001-nZVI were shifted to 1038.70 $cm^{-1}$, 1630.70 $cm^{-1}$, and 3450.96 $cm^{-1}$, respectively, after HA was added, which proved that HA promoted the adsorption of D001-nZVI.

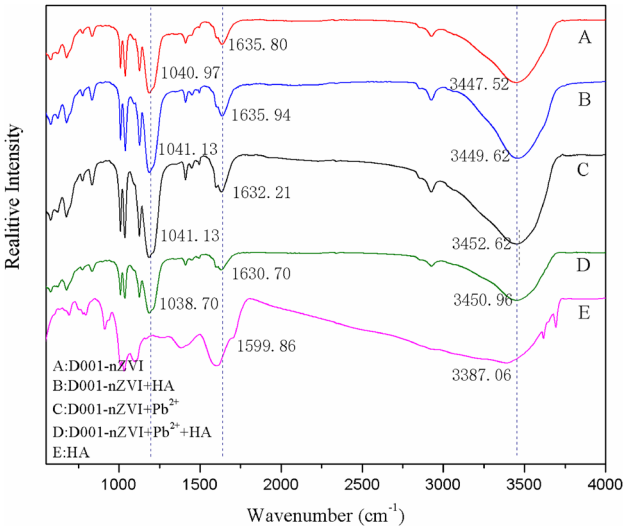


**Figure 3.** FT-IR spectra of (**A**) D001-nZVI; (**B**) D001-nZVI after reacted with 100 mg/L HA; (**C**) D001-nZVI after reacted with 500 ppm $Pb^{2+}$; (**D**) D001-nZVI after reacted with 100 mg/L HA and 500 ppm $Pb^{2+}$; (**E**) HA.

To further investigate the possible sorption mechanism, TEM images of D001-nZVI before and after reaction with HA at low (2 mg/L) and high (100 mg/L) concentration are shown in Fig. 2B. It was found that the addition of HA resulted in nZVI particles with a well-dispersed morphology, and similar results were also obtained in a previous study[25].

The formed HA coating on nZVI was negatively charged, which generated electrostatic repulsion, resulting in well-dispersed nZVI particles. In contrast, when the concentration of HA was low, charge neutralization between HA and the iron oxide surface may cause nZVI particle aggregation, while at high concentrations of added HA, the present steric hindrance and electrostatic repulsion significantly inhibited the aggregation of the particles[44]. Overall, three mechanisms for the HA and $Pb^{2+}$ interaction were found, i.e., HA and $Pb^{2+}$. The complexation of HA and $Pb^{2+}$ as precipitates increased the nZVI reactivity through electrostatic repulsion due to the HA coating and possible adsorption competition between HA and $Pb^{2+}$ on the iron oxide interface. The first two approaches favoured lead ion removal, while the last approach possibly inhibited the $Pb^{2+}$ adsorption.

**Effect of HA on the removal efficiency of $Pb^{2+}$ by D001-nZVI.** Figure 4A shows the effects of different concentrations of HA on the removal of $Pb^{2+}$ by D001-nZVI. The removal efficiency of $Pb^{2+}$ was 97.41% in the absence of HA and gradually decreased with increasing HA addition. In particular, the removal of $Pb^{2+}$ was approximately 90% and remained constant when HA > 30 mg/L. Based on the possible removal mechanisms mentioned, the competitive adsorption of HA and $Pb^{2+}$ dominated the sorption process, leading to a decrease in $Pb^{2+}$ removal. The XRD patterns of D001-nZVI showed different changes in the characteristic diffraction peaks after reacting with $Pb^{2+}$ with HA backgrounds (Fig. 4B). The diffraction peak at 2θ of 29.6° corresponded to the amorphous $Pb(OH)_2$, crystal PbOxH2O morphology corresponding to 2θ at 32.2° and Pb(0), corresponding to 2θ of 55.4° and 62.4°[23,45], which indicated that nZVI could reduce Pb(II) to Pb(0).

The standard reduction potential of Pb(II)/Pb(0) is −0.1263 V, which is higher than the standard reduction potential of Fe(0)/Fe(II) (−0.4402 V)[46]; thus, Pb(II) can easily be reduced by nZVI. Moreover, the iron oxide content and the pH of the solution (Figure S1) also increased slightly during the oxidation of Fe(0) to Fe(II) or/and Fe(III), which was ascribed to the oxidation and hydration of Pb(0) on the surface of D001-nZVI[45]. However, these Fe(0) (2θ = 44.9°) peaks were weakened or disappeared completely in D001-nZVI (Fig. 4B), and the emerging peaks at 34.9° and 36.6° proved the presence of $Fe(OH)_3$ and FeOOH species, respectively. In addition, a strong peak attributed to FeOOH species was detected; when the HA concentration was lower than 2 mg/L, a further increase in the HA concentration led to the transformation of the FeOOH to the $Fe(OH)_3$ species. Similar results were also found in a recent study, in which the presence of Fe(II) ions could promote the conversion of ferrihydrite to FeOOH at room temperature and neutral pH[47]. Therefore, when the concentration of HA was low (< 2 mg/L), the reduction of $Pb^{2+}$ was accompanied by the generation of $Fe^{2+}$, and high amounts of FeOOH were obtained during this stage; the opposite was the case for $Fe(OH)_3$. This was also confirmed by XPS analysis, as shown in Fig. 5. The content of Fe(II) on D001-nZVI after reacting with $Pb^{2+}$ at concentration lower than 2 ppm of HA was reduced, which proved that more $Fe^{2+}$ was involved in the reaction. When the concentration of HA was continuously increased (> 2 mg/L), the surface of nZVI particles continuously adsorbed HA to form the HA coating. As shown in Fig. 5, the content of Fe(II) on D001-nZVI after reacting with $Pb^{2+}$ at concentrations lower than 20 ppm HA remained almost unchanged compared with 0 ppm HA and increased compared with 2 ppm HA. It has been found that some ions or molecules can adsorb on the surface of $Fe(OH)_3$ to inhibit the formation of FeOOH, such as silicate, phosphate, citrate ions and sodium dodecyl sulfate (SDS)[48]. Thus, we concluded that the HA coating on the nZVI surface inhibited the formation of FeOOH, which resulted

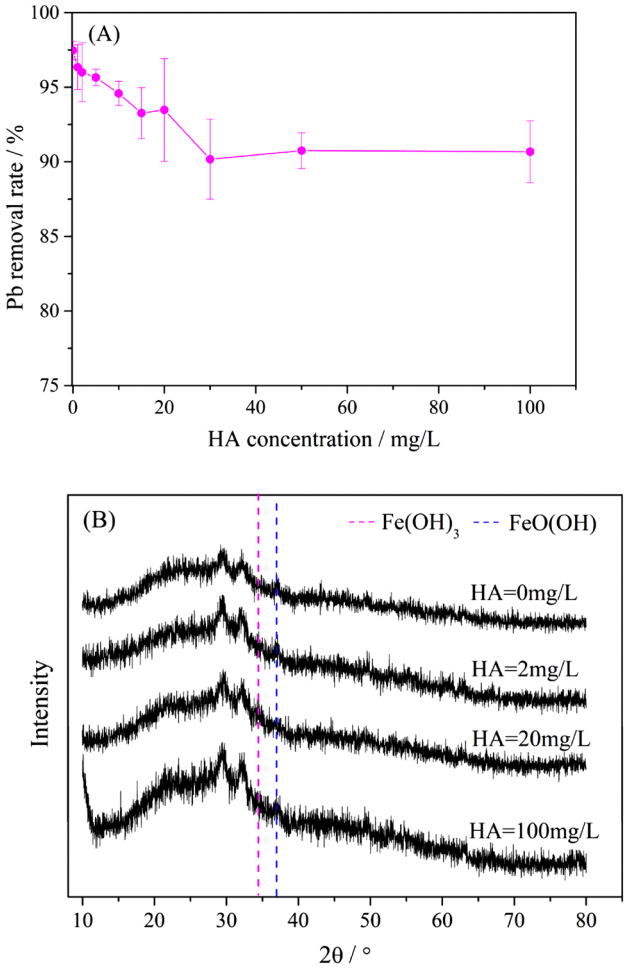


**Figure 4.** nZVI removal characteristics of Pb and changes of its chemical composition: (**A**) Removal rate of lead ions in different concentration of initial HA; (**B**) XRD pattern of D001-nZVI reacted with $Pb^{2+}$ under different concentrations of HA (initial $Pb^{2+}$, 500 ppm; T, 298 K; initial pH, 7; ZVI for all the reaction mixtures was the same and equal to 11.20 Fe% in mass).

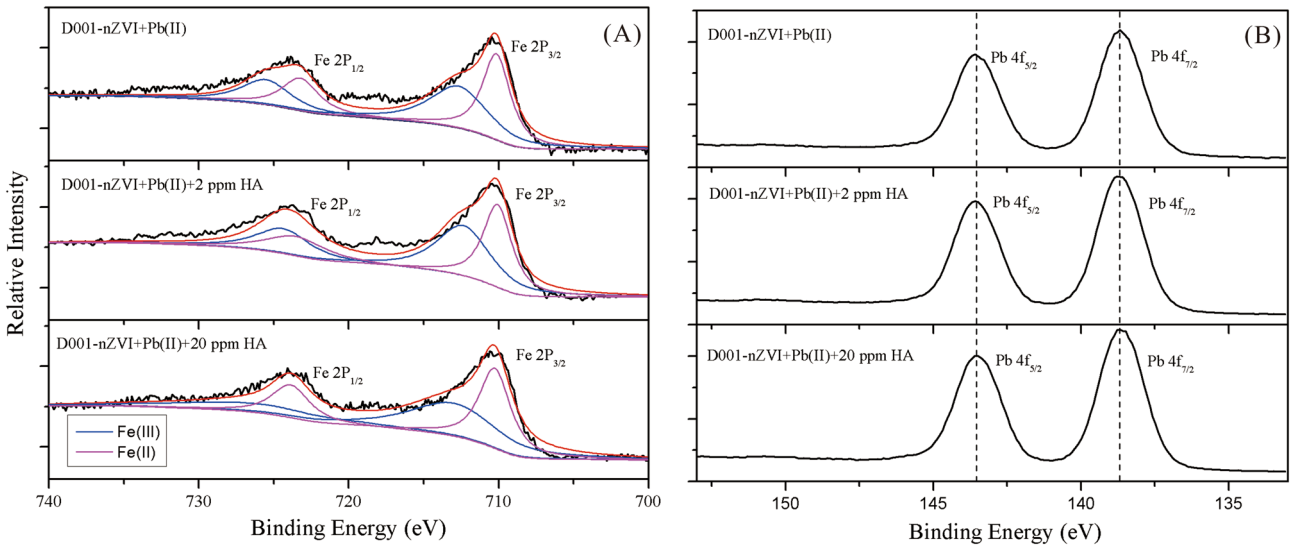


**Figure 5.** XPS spectra for Fe (**A**) and Pb (**B**) on the D001-nZVI after reacted with $Pb^{2+}$ under different concentration of HA (initial $Pb^{2+}$, 500 ppm; T, 298 K; initial pH, 7; HA concentration are 0 ppm, 2 ppm, 20 ppm, respectively).

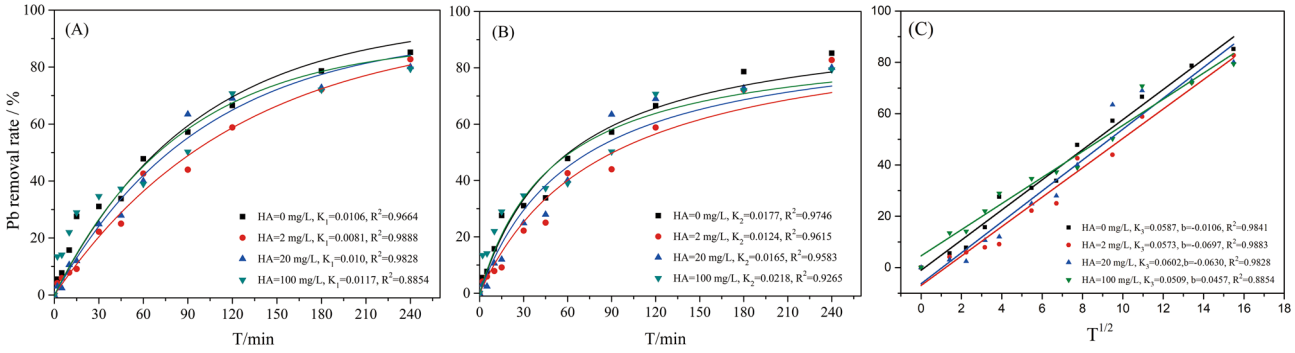


**Figure 6.** The kinetic characteristics of $Pb^{2+}$ removal by D001-nZVI at different concentration of HA: (**A**) the first-order kinetic model curve; (**B**) the second-order kinetic model curve; (**C**) Webber-Morris kinetic model curve.

in a decrease in its content. A previous study also showed that FeOOH can adsorb heavy metal ions[49], which is beneficial to the removal of heavy metal ions; thus, the decrease in FeOOH content may also be one of the reasons for the decrease in the $Pb^{2+}$ removal.

**Effect of HA on the $Pb^{2+}$ removal kinetics.** Kinetic performance is one of the important indicators for evaluating the efficiency of the adsorbent. As shown in Fig. 6, sorption equilibrium was completed in ~ 200 min, and HA addition at different concentrations showed similar sorption behaviours. The relationship between the $Pb^{2+}$ removal rate and the removal time at different HA concentrations was fitted by the first-order kinetic model and the second-order kinetic model, which can be expressed as follows:

$$[C]_t = [C]_e\left(1 - e^{-k_1 t}\right)$$

$$\frac{t}{[C]_t} = \frac{1}{k_2[C]_e^2} + \frac{t}{[C]_e}$$

where $k_1$ and $k_2$ ($min^{-1}$) represent the first-order kinetic reaction constant and the second-order kinetic reaction constant, respectively, and [C]t represents the removal rate of $Pb^{2+}$ in the solution at time t. The fitting parameters of the results are shown in Table S1. The results could be described well by the second-order kinetic model with higher $R^2$ values, and the $[C]_{e,cal2}$ was also closer to $[C]_{e,exp}$ than to $[C]_{e,cal1}$. The value of $k_2$ decreased when the HA concentration increased from 0 to 2 mg/L and may increase to 0.022 when HA > 2 mg/L, which is higher than the value of $k_2$ without HA.

However, the removal rate of $Pb^{2+}$ in the solution conforms to the first-order kinetic model and the second-order kinetic model, and the rate control step cannot be determined. In general, the rate of adsorption kinetics usually depends on three main steps, including external diffusion, intraparticle diffusion, and interaction between the adsorbate and the adsorbents[50]. To determine the actual control steps of the adsorption rate, the results were also analysed by Webber-Morris (intraparticle diffusion model), which describes the overall intraparticle diffusion effect[51,52]. The Webber-Morris (intraparticle diffusion model) can be expressed as follows:

$$[C]_t = k_3 t^{1/2} + b$$

where $k_3$ ($min^{1/2}$) represents the Webber-Morris kinetic reaction constant and b represents the boundary layer index. As shown in Fig. 6C, when the concentration of HA was 0 ~ 20 mg/L, the removal rate of $Pb^{2+}$ was well-fitted by the intraparticle diffusion model, and the correlation coefficients were 0.9828 ~ 0.9883. This result showed that the intraparticle diffusion in the removal process of D001-nZVI to $Pb^{2+}$ was the rate-limiting step at concentrations of 0 ~ 20 mg/L HA. The b values of the removal of $Pb^{2+}$ by D001-nZVI were -0.0697 ~ 0.0457, which were all greater than 0. This result indicated that intraparticle diffusion was not the only rate-limiting process. $Pb^{2+}$ diffusion through the membrane to reach the surface of D001-nZVI also affected the removal.

The concentrations of $Pb^{2+}$ in the solution decreased at low HA concentrations (2 ~ 20 mg/L) due to the complexation of HA and $Pb^{2+}$, indicating that the concentration of $Pb^{2+}$ in the bulk solution decreased, which also led to a dramatic weakening of the concentration driving force. Thus, the external diffusion rate declines. Moreover, the thickness of the particle boundary layer increased due to the HA coating, which also largely limited the internal diffusion of the particles. When the concentration of HA was higher than 20 mg/L, the complexation of HA and $Pb^{2+}$ was no longer dominant; at this time, $Pb^{2+}$ diffusion through the membrane to reach the surface of D001-nZVI controlled the sorption process.

**The fate of $Pb^{2+}$ after reaction with D001-nZVI.** The removal pathway of $Pb^{2+}$ by D001-nZVI in this experimental system included (1) adsorption of $Pb^{2+}$ by the matrix resin D001; (2) reduction of $Pb^{2+}$ by nZVI; and (3) complexation between HA and $Pb^{2+}$. Therefore, it is necessary to explore the main removal pathway of $Pb^{2+}$ as well as the sorption-reduction mechanism at different concentrations of HA. Figure 7 shows an investigation of the Pb mass balance in the reaction system. It was found that the total Pb mass in the system remained

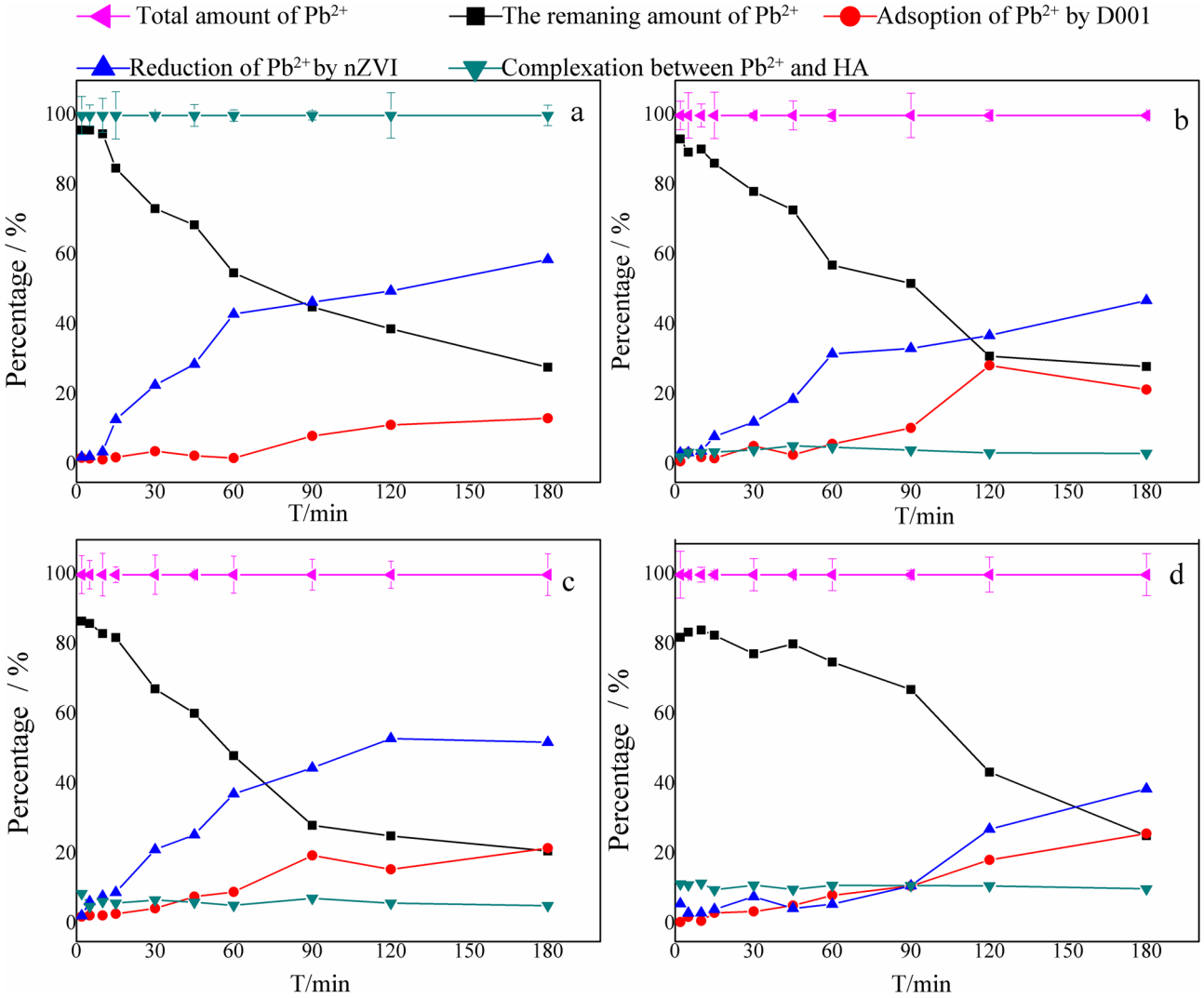


**Figure 7.** The removal of $Pb^{2+}$ by D001-nZVI at different time in different concentration of HA (Figure **a**, **b**, **c**, **d** correspond to HA concentration of 0 mg/L, 2 mg/L, 20 mg/L, 100 mg/L).

at the same level within the error bars and could be correlated with the amount of reduction of $Pb^{2+}$ by nZVI, adsorption of $Pb^{2+}$ by the carrier resin, complexation and the amount of remaining Pb species; the detailed proportions at different concentrations are shown in Fig. 7. The reaction strength order was as follows: reduction of $Pb^{2+}$ by nZVI > adsorption of $Pb^{2+}$ by D001 > complexation of HA and $Pb^{2+}$.

The amount of complex precipitation of $Pb^{2+}$ and HA did not change significantly over time, regardless of whether HA was added. The amount of $Pb^{2+}$ complexation was lower than 0.1% without HA, and when HA = 2, 20 and 100 mg/L, the average amounts of complexation between HA and $Pb^{2+}$ were 3.87%, 6.34% and 10.85%, respectively, and increased with increasing HA concentration. This process promoted the removal of $Pb^{2+}$ to a certain extent.

Overall, the proportion of this fraction was at least twice the amount of adsorption by D001, which indicated that the reduction of $Pb^{2+}$ by nZVI played a major role in the removal of $Pb^{2+}$ by D001-nZVI. Some of the $Pb^{2+}$ removed by nZVI increased over time when HA was added. At the same time points, the amount of removal was 0 mg/L HA > 20 mg/L HA > 2 mg/L HA > 100 mg/L HA. There was a competition between HA and $Pb^{2+}$ for active sites on nZVI, although the HA coating on the nZVI surface results in a better dispersion of the nZVI particles. Therefore, the proportion of $Pb^{2+}$ removed by nZVI decreased with increasing HA. The XRD analysis of Fig. 4B showed that the characteristic peak intensity of FeOOH increased with increasing HA concentration when the HA concentration was lower than 20 mg/L, and FeOOH could adsorb heavy metal ions. Therefore, when the HA concentration was 20 mg/L, the reduction was more efficient than that at HA concentrations of 2 mg/L and 100 mg/L. Moreover, the adsorption amount of $Pb^{2+}$ increased over time after adding different concentrations of HA, and in general, the amount of $Pb^{2+}$ adsorption increased with increasing HA concentration, which indicated that the addition of HA promoted the adsorption of $Pb^{2+}$ on D001. When nZVI was loaded on D001, the positive charge of the oxidation shell surface on nZVI slightly reduced the overall electronegativity of D001-nZVI. After adding HA, the electrostatic attraction between HA and the nZVI oxide shell neutralized

the positive charge and even generated an overall negatively charged surface; thus, the overall electronegativity of D001-nZVI increased, which increased the adsorption of Pb(II).

## Conclusions

In summary, a new nanocomposite, D001-nZVI, was prepared through ion exchange and chemical reduction, and investigated in terms of the HA effects on the removal of $Pb^{2+}$. The result shows that the performance of HA on D001-nZVI removal of $Pb^{2+}$ was related to its concentration. The $Pb^{2+}$ removal rate decreased as the HA concentration increased, but when the HA concentration was greater than 30 mg/L, the $Pb^{2+}$ removal rate remained constant. There were three main mechanisms influencing the reaction process: (1) the complexation between HA and $Pb^{2+}$, (2) the formation of an HA coating due to the adsorption of HA on the surface of nZVI, and (3) competitive adsorption between HA and $Pb^{2+}$ on the iron oxide on the surface of nZVI particles. The former mechanisms two can facilitate the D001-nZVI removal performance, but their effects were all less pronounced than the negative effects caused by the third mechanism. In addition, the adsorption complexation between HA and $Pb^{2+}$ also played a positive role in the removal of $Pb^{2+}$ at higher concentrations of HA. Therefore, in practice, it is necessary to consider the concentration of HA present in the water when nanocomposites are used to remove heavy metal lead ions.

Received: 26 May 2020; Accepted: 27 October 2020
Published online: 12 November 2020

## References

1. Korn, M. *et al.* Talanta, Selective and efficient removal of fluoride from water by in-situ engineered amyloid fibrils-$ZrO_2$ hybrid membranes. *Angew. Chem. Int. Edit.* **69**, 16–24 (2006).
2. Bulletin on Environmental Quality of China's Coastal Waters in 2015. Ministry of Ecology and Environment of the People's Republic of China (2015).
3. Lou, M. T. *et al.* Review on lead pollution in China. *Guangdong Trace Elem. Sci.*. **19**, 15–34 (2012).
4. Fu, F., Wang, Q., Fu, F. & Wang, Q. Removal of heavy metal ions from wastewaters: a review. *J. Environ. Manag.* **92**, 407–418 (2011).
5. Zhang, Q. R. *et al.* Selective and efficient removal of fluoride from water. in situ engineered amyloid fibril/$ZrO_2$ hybrid membranes. *Angew. Chem. Int. Edit.* **58**, 6012–6016 (2019).
6. Jiang, Z. M., Lv, L. & Zhang, W. M. Nitrate reduction using nanosized zero-valent iron supported by polystyrene resins: role of surface functional groups. *Water Res.* **45**, 2191–2198 (2011).
7. Bolisetty, S., Peydayesh, M. & Mezzenga, R. Sustainable technologies for water purification from heavy metals: review and analysis. *Chem. Soc. Rev.* **48**, 463 (2019).
8. Hwang, Y. H., Kim, D. G. & Shin, H. S. Mechanism study of nitrate reduction by nano zero valent iron. *J. Hazard. Mater.* **185**, 1513–1521 (2011).
9. Shi, L. N., Zhang, X. & Chen, Z. L. Removal of chromium (VI) from wastewater using bentonite-supported nanoscale zero-valent iron. *Water Res.* **45**, 886–892 (2011).
10. Jiang, Z. *et al.* Nitrate reduction using nanosized zero-valent iron supported by polystyrene resins: role of surface functional groups. *Water Res.* **45**, 2191–2198 (2011).
11. Ryu, A., Jeong, S. W., Jang, A. & Choi, H. Reduction of highly concentrated nitrate using nanoscale zero-valent iron: effects of aggregation and catalyst on reactivity. *Appl. Catal. B Environ.* **105**, 128–135 (2011).
12. Lv, X., Xu, J., Jiang, G., Tang, J. & Xu, X. Highly active nanoscale zero-valent iron (nZVI)-$Fe_3O_4$ nanocomposites for the removal of chromium(VI) from aqueous solutions. *J. Colloid Interface Sci.* **369**, 460–469 (2012).
13. Kim, S. A. *et al.* Removal of Pb(II) from aqueous solution by a zeolite–nanoscale zero-valent iron composite. *Chem. Eng. J.* **217**, 54–60 (2013).
14. Shi, J., Yi, S., He, H., Long, C. & Li, A. Preparation of nanoscale zero-valent iron supported on chelating resin with nitrogen donor atoms for simultaneous reduction of $Pb^{2+}$ and $NO_3^-$. *Chem. Eng. J.* **230**, 166–171 (2013).
15. Klas, S. & Kirk, D. W. Advantages of low pH and limited oxygenation in arsenite removal from water by zero-valent iron. *J. Hazard. Mater.* **252–253**, 77–82 (2013).
16. Neumann, A. *et al.* Arsenic removal with composite iron matrix filters in Bangladesh: a field and laboratory study. *Environ. Sci. Technol.* **47**, 4544–4554 (2013).
17. Luo, S. *et al.* Synthesis of reactive nanoscale zero valent iron using rectorite supports and its application for Orange II removal. *Chem. Eng. J.* **223**, 1–7 (2013).
18. Shimizu, A., Tokumura, M., Nakajima, K. & Kawase, Y. Phenol removal using zero-valent iron powder in the presence of dissolved oxygen: roles of decomposition by the Fenton reaction and adsorption/precipitation. *J. Hazard. Mater.* **201–202**, 60–67 (2012).
19. Wang, C. *Research on Performance and Mechanism of Removing 210Pb(II) from Aqueous Solution by Coated Nanoscale Zero-Valent Iron* (East China University of Technology, Fuzhou, 2015).
20. Calderon, B. & Fullana, A. Heavy metal release due to aging effect during zero valent iron nanoparticles remediation. *Water Res.* **83**, 1–9 (2015).
21. Karn, B., Kuiken, T. & Otto, M. Nanotechnology and in situ remediation: a review of the benefits and potential risks. *Cienc Saude Coletiva* **16**, 165–178 (2011).
22. Chen, Z. X., Jin, X. Y., Chen, Z., Megharaj, M. & Naidu, R. Removal of methyl orange from aqueous solution using bentonite-supported nanoscale zero-valent iron. *J. Colloid Interface Sci.* **363**, 601–607 (2011).
23. Zhu, H., Jia, Y., Wu, X. & Wang, H. Removal of arsenic from water by supported nano zero-valent iron on activated carbon. *J. Hazard. Mater.* **172**, 1591–1596 (2009).
24. Zhang, X., Lin, S., Chen, Z., Megharaj, M. & Naidu, R. Kaolinite-supported nanoscale zero-valent iron for removal of $Pb^{2+}$ from aqueous solution: reactivity, characterization and mechanism. *Water Res.* **45**, 3481–3488 (2011).
25. Du, Q. *et al.* Bifunctional resin-ZVI composites for effective removal of arsenite through simultaneous adsorption and oxidation. *Water Res.* **47**, 6064–6074 (2013).
26. Shu, H. Y., Chang, M. C., Chen, C. C. & Chen, P. E. Using resin supported nano zero-valent iron particles for decoloration of acid blue 113 azo dye solution. *J. Hazard. Mater.* **184**, 499–505 (2010).
27. He, F. & Zhao, D. Y. Preparation and characterization of a new class of starch-stabilized bimetallic nanoparticles for degradation of chlorinated hydrocarbons in water. *Environ. Sci. Technol.* **39**, 3314–3320 (2005).
28. Dong, H. & Lo, I. M. Influence of humic acid on the colloidal stability of surface-modified nano zero-valent iron. *Water Res.* **47**, 419–427 (2013).

29. Jiang, L. L. *et al.* Nitrate reduction using nanosized zero-valent iron supported by polystyrene resins. *Water Res.* **45**, 2191–2198 (2011).
30. Chanthapon, N., Sarkar, S., Kidkhunthod, P. & Padungthon, S. Lead removal by a reusable gel cation exchange resin containing nano-scale zero valent iron. *Chem. Eng. J.* **331**, 545–555 (2018).
31. Xu, J. *et al.* Promotion effect of $Fe^{2+}$ and $Fe_3O_4$ on nitrate reduction using zero-valent iron. *Desalination* **284**, 9–13 (2012).
32. Saleh, N. *et al.* Ionic strength and composition affect the mobility of surface-modified Fe0 nanoparticles in watersaturated sand columns. *Environ. Sci. Technol.* **42**, 3349–3355 (2008).
33. Liu, T., Rao, P. & Lo, I. M. C. Influences of humic acid, bicarbonate and calcium on Cr(VI) reductive removal by zero-valent iron. *Sci. Total Environ.* **407**, 3407–3414 (2009).
34. Zhou, X. P. *New technology and Application of Humic Acid* (Chemical Industry Press, Beijing, 2015).
35. Sposito, G. Sorption of trace-matals by humic materials in soils and natural-waters. *C R C Crit. Rev. Environ. Control* **16**, 193–229 (1986).
36. Wang, Q., Cissoko, N., Zhou, M. & Xu, X. Effects and mechanism of humic acid on chromium(VI) removal by zero-valent iron (Fe0) nanoparticles. *Phys. Chem. Earth Parts A/B/C* **36**, 442–446 (2011).
37. Seunghun Kang, B. X. Humic acid fractionation upon sequential adsorption onto goethite. *Langmuir* **24**, 2525–2531 (2008).
38. Liu, J. F., Zhao, Z. S. & Jiang, G. B. Coating $Fe_3O_4$ magnetic nanoparticles with humic acid for high efficient removal of heavy metals in water. *Environ. Sci. Technol.* **42**, 6949–6954 (2008).
39. Gupta, V. K. & Nayak, A. Cadmium removal and recovery from aqueous solutions by novel adsorbents prepared from orange peel and $Fe_2O_3$ nanoparticles. *Chem. Eng. J.* **180**, 81–90 (2012).
40. Wang, L., Zhou, H., Liu, J., Chen, J. & Jiang, Z. Effect of humic acid on the nitrate removal by strong base anion exchanger supported nanoscale zero-valent iron composite. *Water Air Soil Pollut.* **229**, 357 (2018).
41. Kanel, S. R., Manning, B., Charlet, L. & Choi, H. Removal of arsenic(III) from groundwater by nanoscale zero-valent iron. *Environ Sci Technol* **39**, 1291–1298 (2005).
42. Illés, E. & Tombácz, E. The role of variable surface charge and surface complexation in the adsorption of humic acid on magnetite. *Colloid Surf. A* **230**, 99–109 (2003).
43. Li, X. & Shang, C. Role of humic acid and quinone model compounds in bromate reduction by zerovalent iron. *Environ. Sci. Technol.* **39**, 1092–1100 (2005).
44. Vindedahl, A. M., Strehlau, J. H., Arnold, W. A. & Penn, R. L. Organic matter and iron oxide nanoparticles: aggregation, interactions, and reactivity. *Environ. Sci. Nano* **3**, 494–505 (2016).
45. Ponder, S. M., Darab, J. G. & Mallouk, T. E. Remediation of Cr(VI) and Pb(II) aqueous solutions using supported, nanoscale zero-valent iron. *Environ. Sci. Technol.* **34**, 2564–2569 (2000).
46. Uezuem, C. *et al.* Synthesis and characterization of kaolinite-supported zero-valent iron nanoparticles and their application for the removal of aqueous $Cu^{2+}$ and $Co^{2+}$ ions. *Appl. Clay Sci.* **43**, 172–181 (2009).
47. Cornell, S. U. & Taylor, R. M. *The Iron Oxides* (VCH Publishers, New York, 1996).
48. Saric, A., Music, S., Nomura, K. & Popovic, S. Microstructural properties of Fe-oxide powders obtained by precipitation from $FeCl_3$ solutions. *Mater. Sci. Eng. B Solid* **56**, 43–52 (1998).
49. Xiong, H. *Synthesis of Different Crystalline Iron Oxyhydroxides and Their Roles in Adsorption and Removal of Cr(VI) Solution* (Nanjing Agrieultural University, Nanjing, 2008).
50. Shuang, C., Wang, M., Zhou, Q., Zhou, W. & Li, A. Enhanced adsorption and antifouling performance of anion-exchange resin by the effect of incorporated $Fe_3O_4$ for removing humic acid. *Water Res.* **47**, 6406–6414 (2013).
51. Yang, G. *et al.* Removal of congo red and methylene blue from aqueous solutions by vermicompost-derived biochars. *PLoS ONE* **11**, 0154562 (2016).
52. Lu, C. P. *Study on the Synthesis of Magnetic Polystyrene Based Macroporous Resins and Their Adsorption Performance to Metal Ions in Aqueous Solution* (Lanzhou University of Technology, Lanzhou, 2011).


## Acknowledgments

This research is supported by the National Key Research and Development Program of China (2018YFD0800604), the Natural Scientific Foundation of China (Grant No. 21207110) and Fundamental Research Funds for the Central Universities (XDJK2018B045).

## Author contributions

Conceptualization: L.W., Z.J.. Data curation: L.W. Formal analysis: Z.J. Funding acquisition: Z.J., S.W. Investigation: L.W., S.W. Methodology: L. W., Z.J. Project administration: Z.J.. Resources: L.W., S.W. Supervision: Z.J. Writing-original draft: L.W.. Writing-review and editing: L.W., Z.J.

## Competing interests

The authors declare no competing interests.

## Additional information

**Supplementary information** is available for this paper at https://doi.org/10.1038/s41598-020-76362-1.

**Correspondence** and requests for materials should be addressed to Z.J.

**Reprints and permissions information** is available at www.nature.com/reprints.

**Publisher's note** Springer Nature remains neutral with regard to jurisdictional claims in published maps and institutional affiliations.